94

N91-23007

PRE-TERRESTRIAL ORIGIN OF "RUST" IN THE NAKHLA METEORITE.

Susan J. Wentworth[1] and James L. Gooding[2], [1]Lockheed/ESC, 2400 NASA Rd. 1, Houston TX 77058. [2]SN21/Planetary Science Branch, NASA/Johnson Space Center, Houston, TX 77058.

INTRODUCTION. As part of our campaign to identify and rigorously test evidence for aqueous geochemistry in shergottite, nakhlite, and chassignite (SNC) meteorites, we previously reported evidence for pre-terrestrial origin of calcium carbonate associated with silicate "rust" in Nakhla [1]. Here we present quantitative elemental compositions and summarize textural evidence for pre-terrestrial origin of the rust. We denote the material in question as "rust" because its phase composition remains unknown. The rust is probably the same as the iddingsite-like material reported by Bunch and Reid [2] and might be related to pockets of material called "brownies" by Papanastassiou and Wasserburg [3].

SAMPLES AND METHODS. Although our previous work on Nakhla [1,4,5] has also involved untreated interior and exterior chips obtained from the British Museum (Natural History), all data reported here were obtained from polished thin sections prepared from Nakhla specimen, USNM-426 (Smithsonian Institution). Scanning electron microscopy (SEM) and energy-dispersive X-ray spectrometry (EDS) followed our previously described procedures and included mineral-standardized, quantitative EDS analyses. Relative to conventional wavelength-dispersive microprobe analyses, our method permitted beam-spot sizes of 1-10 μm, as necessitated by the rust occurrences.

RESULTS AND DISCUSSION. *MICROSTRATIGRAPHY.* Compelling evidence for pre-terrestrial origin of the rust is found as rust veins truncated by fusion crust (Fig. 1) and preserved as faults in sutured igneous crystals (Fig. 2). Rust veins that approach the meteorite's fusion crust become discontinuous and exhibit vugs that suggest partial decrepitation; no rust veins that penetrate fusion crust have been found. Because the rust probably contains volatile compounds (see below), it is reasonable to expect that heating near the ablation surface (formed during atmospheric entry to Earth) would encourage devolatilization of the rust. Hence, absence of rust veins in fusion crust and vugs in rust veins near fusion crust (but not at distance from fusion crust) clearly imply that the rust existed in the meteorite before atmospheric entry. At least one unmistakable example of a vein post-dated by later endogenous events occurs as a faulted rust vein enclosed in an olivine crystal (Fig. 2). It is obvious that the rust vein has been broken by a fault but the two disjointed sections of the vein are separated by clear olivine rather than an open fracture. We infer that, after faulting, the fracture was at least partially healed by elevated pressure. It is difficult to conceive any reasonable natural processes that would break and suture an igneous mineral after the meteorite arrived on Earth. Accordingly, disturbance of the rust vein must have occurred before the meteorite arrived on Earth and, most likely, on the Nakhla parent planet. *COMPOSITION.* Our results for the average elemental composition of the rust (Table 1) generally agree with those of Bunch and Reid [2] except for Al and Na. Compared with the earlier data [2], we find much lower Al. Because our analyses of Al in Nakhla plagioclase and pyroxene agree with the respective data of Bunch and Reid [2], no systematic analytical error is suspected in our Al data. Our Na results for plagioclase agree with those of Bunch and Reid [2] but are systematically high relative to reference samples that contain very minor to trace Na. We conclude that the rust actually contains < 1% Na_2O. Low analytical totals, both in

Table 1. Elemental compositions (weight percent) of rust in Nakhla determined by electron probe microanalysis (all iron calculated as Fe_2O_3; EDS background problem makes our Na results systematically high; nr = not reported).

	SiO_2	TiO_2	Al_2O_3	Cr_2O_3	Fe_2O_3	NiO	MnO	MgO	CaO	Na_2O	K_2O	P_2O_5	SO_3	Cl	Total
Avg. of 78 spots	40.21	0.02	0.74	0.03	37.93	< 0.01	0.63	6.82	1.14	(1.16)	0.60	0.06	0.14	0.66	90.13
Standard deviation	3.66	0.03	0.31	0.03	4.68	0.01	0.26	0.71	1.51	(0.37)	0.17	0.09	0.12	0.33	
(this work)															
Unknown "iddingsite" (Bunch and Reid [2])	43.6	nr	5.8	nr	30.56	nr	0.37	9.4	0.73	0.21	0.10	nr	nr	nr	90.77

our data and in those of Bunch and Reid [2], suggest that the rust contains water. Although admixed carbonate occurs in some places [1], carbon contents in carbonate-free areas are near background levels and do not contribute significantly to the deficit. Intrinsic sulfur is very low except in those places where admixed calcium sulfate is found. Chlorine, however, is a characteristic component that is not correlated with known occurrences of sodium chloride. The fluids that deposited the rust probably carried chloride that was not indigenous to the igneous-rock parent of Nakhla. Absence of significant interelemental correlations implies that the rust is a single phase with compositional heterogeneities at the scale of 1-10 μm. Poor crystallinity was previously inferred from a preliminary transmission electron microscopy (TEM) study [6]. In terms of a single-phase model, structural-formula calculations by the method of Gooding [7] show that our average rust composition gives nearly equal goodness-of-fit values for dioctahedral smectite and stilpnomelane. By definition, genuine iddingsite (a smectite-goethite mixture), would contain smectite as a major component. New high-resolution TEM analyses are needed to verify whether the rust is crystalline or mostly a colloidal gel.

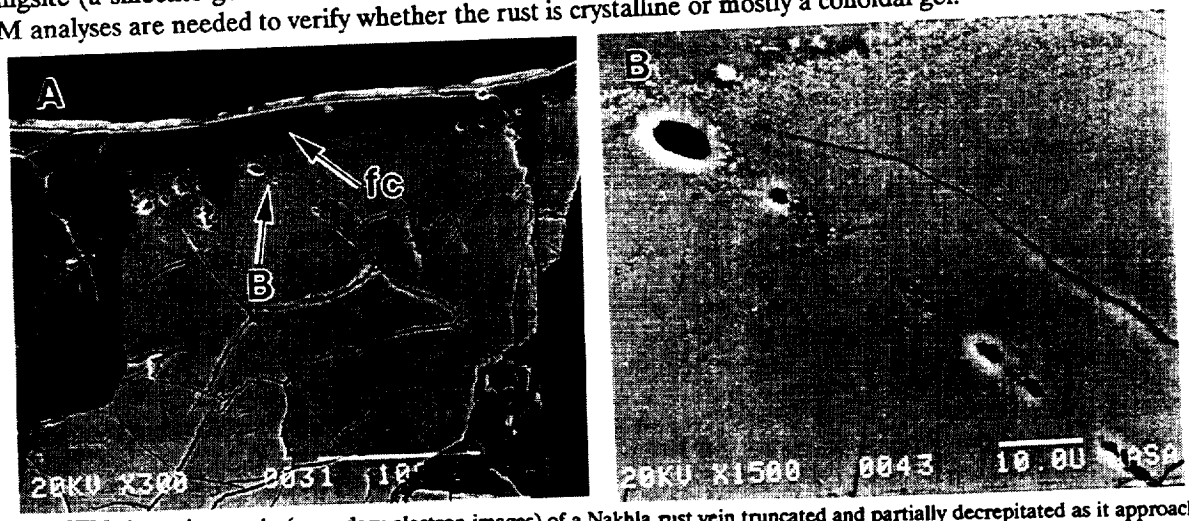

Figure 1. SEM photomicrographs (secondary-electron images) of a Nakhla rust vein truncated and partially decrepitated as it approaches fusion crust (fc). Scale bars are in micrometers.

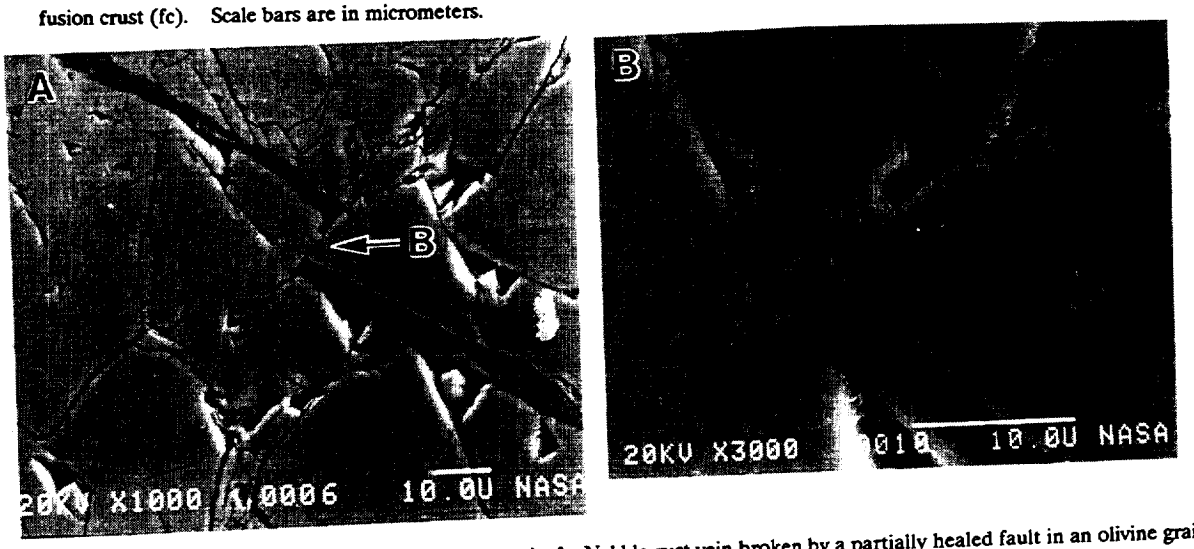

Figure 2. SEM photomicrographs (secondary-electron images) of a Nakhla rust vein broken by a partially healed fault in an olivine grain. Frame (B) is a detailed view of the area marked by an arrow in (A). Scale bars are in micrometers.

References. [1] Wentworth S. J. and Gooding J. L. (1989) *Lunar Planet. Sci XX*, LPI, Houston, p. 1193-1194. [2] Bunch T. E. and Reid A. M. (1975) *Meteoritics, 10*, p. 303-315. [3] Papanastassiou D. A. and Wasserburg G. J. (1974) *Geophys. Res. Lett., 1*, p. 23-26. [4] Wentworth S. J. and Gooding J. L. (1988) *Lunar Planet. Sci. XIX*, LPI, Houston, p. 1261-1262. [5] Wentworth S. J. and Gooding J. L. (1988) *Meteoritics, 23*, p. 310. [6] Ashworth J. R. and Hutchison R. (1975) *Nature, 256*, p. 714-715. [7] Gooding J. L. (1985) *Lunar Planet. Sci. XVI*, LPI, Houston, p. 278-279.

A MODEL FOR CRUSTAL SUBDUCTION BY LARGE IMPACTS; R. W. Wichman and P. H. Schultz, Dept of Geological Sciences, Brown University, Providence, R.I. 02912.

Introduction: In the standard model of crater excavation, ballistically ejected material represents only about half the volume of the transient cavity (1). The other half corresponds to downwardly displaced, shock-compressed material driven beneath the transient cavity (e.g., 1, 2, 3, 4, 5). In large craters, the final crater then forms by the collapse of this transient cavity with uplift and inward flow of the shocked, displaced material comprising the crater floor (6). Although this idealized model of crater formation fits most well-preserved planetary impact structures, it implicitly assumes an elastic halfspace beneath the target surface which may be inappropriate for modeling the largest early basin-forming impacts. For these very large impacts, the depth of the transient cavity may excede the lithospheric thickness and, at least on Mars, such cavities apparently can interact with underlying viscous mantle regimes during basin formation (7). The extreme size of these cratering events also challenges some of the assumptions concerning cavity growth and collapse extrapolated from smaller structures (8). In this abstract, we propose that viscous deformation beneath very large impacts can allow emplacement of vertically displaced crustal material in the mantle, and we speculate on the implications such "impact subduction" might have for subsequent mantle evolution.

Subduction Model: Although material flow fields result in ballistic trajectories for most near-surface regions of the transient cavity, a full target section is preserved under the center of the impact. In the case of an elastic half space, compression of this section against undeformed rocks at greater depth enhances lateral flow, disrupting the column and spreading it across the base of the transient cavity. If viscous flow occurs beneath the impact, however, downward displacement of this crustal section is partly accomodated by lateral flow in the mantle below. This process transfers impact deformation from the lithospheric section to the mantle and results in the emplacement of shocked crustal material into rocks of the upper mantle or asthenosphere. Although later dynamic rebound might limit the depths such material could reach, rebound uplifts the region beneath the crater as a whole (not the displaced elements of the transient cavity alone) and the sub-impact crustal section initially should stay in the mantle.

Viscous deformation of the mantle during impact is thus a necesary condition for the emplacement of crustal sections at depth. The probability of such deformation can be evaluated by comparing the duration of the impact event to the Maxwell time (T_m) of the mantle: $T_m = \tau/2\mu\,\dot{\epsilon}$ where τ is applied shear stress, μ is shear modulus (~ 10^6 MPa) and $\dot{\epsilon}$ is strain rate of deformation. The Maxwell time is defined as the time required for viscous creep under stress to equal elastic strain (9); consequently, viscous behavior occurs when deformation times are greater than T_m. Deformation is essentially elastic for timescales less than T_m (9). If an impact generates shear stresses of over 10 kilobars (10^3 MPa), strain rates in an olivine mantle range from 10^{-2} to 10^{-4} /s for mantle temperatures of 800–1000°C (10). These values translate to Maxwell times on the order of 1–100 seconds. Because mantle flow requires that the duration of impact exceed T_m, only large, low-velocity (5–6 km/s) impactors (which have impactor penetration times of several tens of seconds (8)) are likely to induce such a viscous mantle response.

The extent of viscous deformation beneath an impact depends on the impact angle and the duration of the impact relative to T_m. If we define d as the depth of the transient cavity (roughly the penetration depth of the projectile into the target), for near-vertical (>60°) impacts, d can be approximated by the projectile diameter (D_p) but d decreases significantly as the impact angle is then reduced to 5° (11). While rare, near-vertical impacts are not improbable and are the most likely to emplace material at depth in the mantle. For a near-vertical impact with a duration equal to T_m, therefore, we expect viscous mantle deformation comparable to the size of the impact cavity extending to depths of ~D_p beneath the base of the transient cavity. Since the thickness of the down-driven core is of the same scale as the mantle deformation, the crustal section remains near the base of the transient cavity and is likely to be embedded in the basin floor after dynamic rebound. If the duration of the impact is significantly greater than T_m, however, lithospheric material can penetrate the mantle to depths of several D_p. We propose that mantle flow will engulf this displaced crustal section outright with depths of crustal burial in the range of ~ $0.5D_p$ to $2D_p$. This burial of crustal material in the mantle is reminiscent of terrestrial plate subduction and, for a projectile 200 km in diameter, such "subduction" could bury crust to depths of between 100 and 400 km.

The requirement of large, low-velocity impacts for this subduction mechanism limits the extent of this process in planetary history. First, impacts of sufficient size are restricted to the period of basin-forming impacts before ~3.7 Ga. The low impact velocity, however, is a stronger constraint on the occurrence of impact subduction, since only a few planetary impactor populations permit impacts at 5–6 km/s. The planet most likely to have experienced such collisions is Mars, where impact velocities range down to ~5 km/s for co-orbiting, heliocentric objects (12). The coincidence in age of these basins with a time of predicted high mantle temperatures (13) also favors subduction by this mechanism. On the Earth and Venus, impact velocities range from 15–40 km/s and 17–44 km/s, respectively (8,14) and impact subduction is much less likely. Although viscous deformation beneath the impact is still possible at velocities of 15 km/s (for mantle temperatures on the order of

1300–1400°), the increased extent of of vaporization and melting beneath the impact may preclude preservation of a lithospheric section in the mantle during cavity collapse. Some contamination of the mantle by projectile or crustal components might still be expected, however. On Mercury, the predicted impact velocities for comets and earth-crossing asteroids (~34–44 km/s (8)) probably preclude impact subduction. Nevertheless, impactors from the postulated population of Vulcan asteroids (15) should have had much lower velocities, so impact subduction is also possible for Mercury. The probability of subduction on the Moon (impact velocities down to ~6 km/s (12)), depends more strongly on the state of the lunar interior. Thinner lithospheres associated with a magma ocean might permit early subduction events, but the growth of the lithosphere over time would inhibit mantle flow and prevent later subduction.

Implications: Unlike the more continuous subduction of oceanic plates observed on Earth, impact subduction is randomly located and episodic on a global scale. Hence only random and isolated regions of a planetary mantle can be modified by this process. Long-term effects of oceanic subduction such as repeated passage of melts into island arcs or convection beneath back arc basins are thus unlikely to occur for impact subduction. In further contrast, mantle cooling associated with subduction of cold lithospheric plates should not occur with impact subduction due to both shock heating and shear deformation in the subducted section. To first order, this section is presumed to be in thermal equilibrium with normal mantle temperatures at the time of emplacement. Although such a view is over simplistic, the mantle evolution sequence presented below can be regarded as indicative of the relative time scales required to achieve various mantle states.

Impact subduction can potentially influence mantle evolution in two ways. Injection of crustal radiogenic elements into the mantle could affect the long-term thermal history, whereas the introduction of crustal volatiles could affect the melting sequence. In the first case, a crustal block would begin to melt in ~4–6 Ma for subduction to 10 kb pressure with an initial post-impact temperature of 1000°C. Total equilibrium melting then would occur in 9–11 Ma. Significant mantle melting is unlikely to result in this time, since ~16 Ma are needed to achieve lherzolite melting temperatures outside a subducted crustal block. The melting of embedded crustal material, however, will influence the long term thermal evolution of the surrounding mantle. Since a fraction of melt is trapped along grain boundaries during porous flow, we can approximate the mantle composition after crustal melting by mixing a disseminated crustal component into the mantle. For mantle-crust ratios of 100:1, such mixing can double the abundance of heat producing elements in the mantle and these added heat sources eventually can induce mantle partial melts some 100–500 Ma after the subduction event.

The subduction of volatile concentrations could produce mantle melts on much shorter time scales. Although water is unlikely to be a major constituent of the crustal section as a whole, water or ice may be concentrated in near surface regions. For a volatile-rich regolith 500 m thick with 25% porosity, subduction under a 100-km radius projectile can subduct over 1000 km^3 of water. If the projectile caps the subducted section and drives it into the mantle, this volatile phase may not escape into the transient cavity and will be trapped instead near the top of the crustal section. Addition of such a vapor phase to surrounding mantle compositions significantly reduces the solidus temperatures and, at 1000°C and 10 kb, can initiate immediate mantle melting. If carbonates are present in the martian regolith, the associated fluid-rich and volatile phases could possibly acheive a kimberlitic character.

Conclusions: Large, low velocity impacts may inject significant crustal sections into a planetary mantle, but this process will be most efficient if the mantle yields viscously around impact-driven subsidence. Such behavior is most likely before 3.7 Ga on Mars, but also may have occurred on Mercury or the early Moon. The depth of subduction is dependent on the relative scale of impact and mantle flow regimes, but can achieve depths of over 100–200 km for projectiles over 100 km in radius. The effects of such subduction on mantle evolution are unlike those observed in terrestrial subduction zones and primarily reflect the effects of subducted volatile and radiogenic isotope concentrations. Escape of vapor into the mantle should produce kimberlite-like mantle melts soon after impact. Crustal melts develop some 5–10 Ma after impact and enrich higher mantle regions in radiogenic isotopes. Finally, isotopic heating of this enriched mantle may lead to renewed mantle melting several hundred million years after the original impact event. Such a mantle melt sequence may fit the general sequence of highland volcanism observed on Mars where explosive, patera volcanism evidently preceded formation of most of the basaltic shields and ridged plains (16).

REFERENCES: 1) Stoffler et al (1975) *J. Geophys. Res. 80*, p. 4062–4077. 2) Gault et al (1968) In *Shock Metamorphism of Natural Materials* (R.M. French and N.M. Short, eds.) p. 87–99. 3) Dence et al (1977) In *Impact and Explosion Cratering* (D.J. Roddy, R.O. Peppin and R.B. Merrill, eds.) p. 247–275. 4) Schultz et al (1981) *Proc. Lunar Planet. Sci. 12A*, p. 181–195. 5) Croft (1981) *Proc. Lunar Planet. Sci. 12A*, p. 207–225. 6) Grieve (1981) *Proc. Lunar Planet. Sci. 12A*, p. 37–57. 7) Wichman and Schultz (1989) *J. Geophys. Res. 94*, 17333–17357. 8) Schultz (1988) In *Mercury* (F. Villas, C.R. Chapman and M.S. Matthews, eds.) p. 274–335. 9) Melosh (1989) *Impact Cratering*, p. 156. 10) Stocker and Ashby (1973) *Rev. Geophys. Space Physics 11*, p. 391–426. 11) Gault and Wedekind (1978) *Proc. Lunar Planet. Sci. Conf. 9*, 3843–3875. 12) Hartmann (1977) *Icarus 31*, 260–276. 13) Schubert et al (1979) *Icarus 38*, 192–211. 14) Shoemaker (1977) *Impact and Explosion Cratering* (Roddy, D.J., Peppin, R.D., and Merrill, R.B., eds) pp. 617–628. 15) Leake et al (1987) *Icarus 71*, 350–375. 16) Grecley and Spudis (1981) *Rev. Geoph. Space Phys. 19*, 13–41.

LARGE SCALE COMPRESSION STRUCTURES IN THE ERIDANIA–PHAETHONTIS REGION: MORE EVIDENCE FOR POLAR WANDERING. R. W. Wichman and P. H. Schultz, Dept. of Geological Sciences. Brown University, Providence R.I.

INTRODUCTION: Although most tectonic structures on Mars can be associated with stresses due to either Tharsis formation (1,2,3,4) or basin modification (4,5,6), some structures in the martian highlands appear to be independent of both stress sources. Two major systems of ridges and scarps rival the lobate scarps of Mercury in size and indicate that a large, regional–scale compressional event occurred in the Terra Cimmeria/Terra Sirenum region (7). These structures cannot be explained by either Tharsis–centered or basin–centered regional stress models, but may reflect deformation due to polar wandering as predicted by Melosh (8). If the Tharsis Province was not so interesting tectonically, the size and isolation of these features would have attracted immediate attention and possibly stimulated discussions comparable to those of the mid–1970's for Mercury. In this abstract, we use crater deformation to estimate the amount of crustal shortening across these scarp/ridge systems and reconsider the possible sources the causative compressional stress field.

FEATURE DESCRIPTION: The ridge systems described here are Eridania Scopulus and a system of scarps and ridges located near the Copernicus impact basin. The two systems are of similar age with crater dates (derived from linear crater counts (6,9)) of ~381 ± 270 and ~341 ± 240 $N(>5)/10^6$ km^2, respectively. The Copernicus ridge system is at least 840 km in length, whereas Eridania Scopulus extends over 1000 km. Shadow measurements indicate typical scarp and ridge heights of 500–700 m with a maximum relief exceeding 1 km. The systems are thus comparable in size and scale of deformation to the mercurian lobate scarps, which are typically several hundreds of kilometers in length and range in relief from a few hundreds of meters to one or two kilometers (10,11). The martian systems differ, however, in detailed morphology from the mercurian lobate scarps. The mercurian scarps are typically more rounded and flatter in profile than the martian features; and while the mercurian scarps occur as long, individual features, the martian systems are continuous bands of deformation 100 to 200 km wide containing between 2 and 5 distinct, parallel to subparallel structures. In general, these structures are scarp–like with a backslope away from the scarp on the uplifted side. Where they cross the floors of large craters (>20 km diameter) or intercrater plains units, scarp expression is subdued and more rounded. In some plains regions the scarps then merge into wrinkle ridge systems of the same orientation. Finally, the martian scarp systems coincide with or form apparent linear topographic highs (figure 1). Such behavior is not characteristic of the mercurian lobate scarps and may reflect the combined effects of uplift across individual structures in the martian systems.

CRUSTAL SHORTENING: The nature and degree of deformation in the martian ridge/scarps are best revealed by the modification of craters. Deformation most commonly joins scarps of higher relief on each side of the crater with a linear, asymmetric ridge cutting directly across the crater floor. This pattern resembles crater deformation along the mercurian lobate scarps (11), but differs from the typical deformation associated with smaller wrinkle ridges, which tend to curve around a crater interior instead of cutting directly across it (4,12). A less common modification along the martian ridge/scarps preserves partial craters on the elevated side of a scarp but does not preserve the corresponding down–thrown rim sections (figure 1). Three craters appear foreshortened due to compressional deformation; one of these also shows an offset rim along the scarp resembling deformation of the Guido d'Arezzo crater by the Vostok scarp on Mercury (11). For initially circular craters with no extension perpendicular to compression, the difference between the long and short axes of a deformed crater provides a measure of the regional shortening across the structure. Such measurements for these three craters indicate on the order of 1.5–3 km of crustal shortening across individual scarp features. This is comparable to the values derived by Strom et al (10) for Mercury, where approximately 1–2 km of shortening is estimated for individual mercurian lobate scarps.

The linear nature of deformation in crater interiors and the preservation of uplifted partial craters are consistent with compression by deep–seated thrust or reverse faulting. Consequently, the observed scarp relief helps to constrain fault models for comparison with the observed crater shortening. For a reverse fault with a dip of 60° and a scarp 500 m in elevation, we would expect ~290 m of shortening, a value some 5 to 10 times smaller than that indicated by the deformed craters. Alternatively, a thrust fault with a dip of 25° and scarp relief of 500 m would indicate ~1000 m of shortening, consistent with the estimated crater deformation. Therefore, a thrust fault model for these scarps appears consistent with the observed deformation, and the parallel scarps in the Eridania and Copernicus–Newton systems might represent systems of associated thrust sheets. If the shortening over each thrust is on the order of 1–2 km, in keeping with the crater deformation, such systems could accomodate up to 5 to 10 km of regional shortening perpendicular to the scarp trends.

DISCUSSION: The timing of this compressional event can be derived from the crater ages of the two systems and is broadly correlated to the time of Tharsis formation (figure 2). Due to the large error bars, however, these age determinations encompass both the time of ancient Tharsis faulting and the later main phase of Tharsis radial fracturing. Although coincident in time with Tharsis–centered

deformation, the scarp/ridge systems occur over 70° from the center of Tharsis. Of the Tharsis load models developed by Banerdt et al (3), only the isostatic load model could provide compressive stresses at this distance from Tharsis. Based on the observed deformation east of Tharsis, however, Banerdt et al argue that this model only applies to regions less than 40° from the Tharsis center. Furthermore, the two scarp/ridge systems occur at a distinct angle to each other; neither trend is consistent with the Tharsis stress orientations. Because the systems are well removed from the nearest recognized large impact basins (Hellas, Isidis), basin-centered stresses also seems negligible. Even if a large buried basin did exist in the region, current models of basin-centered deformation (6) could not account for the observed pattern of regional compression.

Some significant regional stress field independent of both Tharsis and basin-controlled deformation thus appears responsible for the formation of these ridge/scarp systems. The global contraction mechanism proposed for Mercury (10,11) seems unlikely on Mars given the early timing and regional scale of the ridge/scarps as well as the widespread contemporary extension associated with Tharsis. Polar wandering, however, can simultaneously produce regions of compressive and tensile stress at the several kilobar level (8), thereby producing the scale of deformation indicated by the crater shortening data. The location and orientation of the scarp/ridge systems are consistent with polar wandering in response to Tharsis development (7), as is the correlation in age of ridge formation with initial Tharsis activity.

CONCLUSIONS: Large ridge/scarp systems in the Terra Cimeria/Terra Sirenum region appear to reflect a major regional event of compressional deformation with regional crustal shortening of up to 5–10 km. Although contemporary with Tharsis fracturing, ridge system formation appears to be independent of Tharsis stress fields and is more consistent with deformation expected in the polar wander scenario of Schultz and Lutz (7).

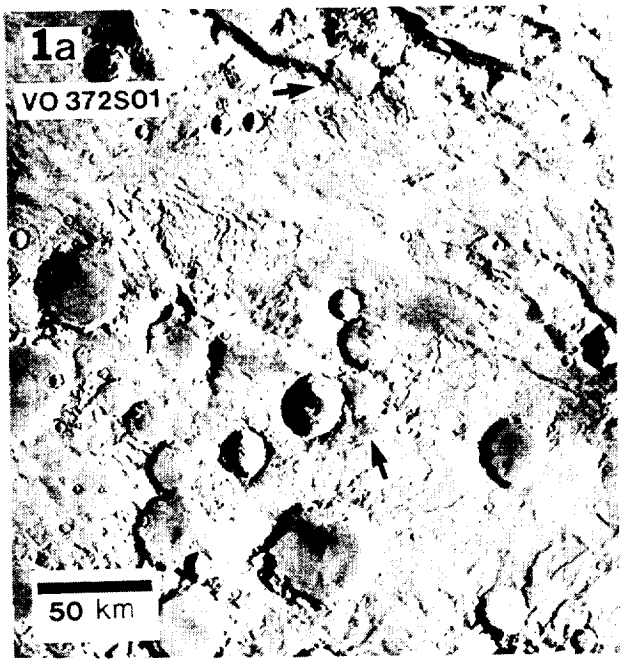

Figure 1. Parts of the Copernicus system (a) and Eridania Scopulus (b). Arrows indicate craters modified by scarp formation.

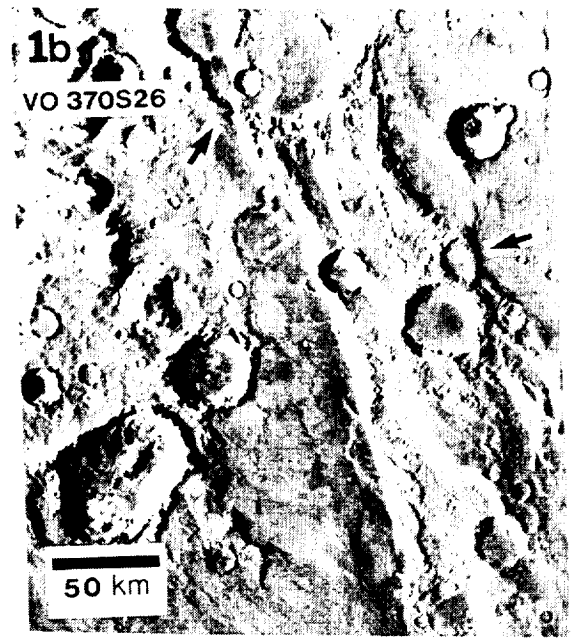

REFERENCES: 1)Wise et al (1979) *Icarus 38*, 456-472. 2)Plescia and Saunders (1982) *J. Geoph. Res. 87*, 9775-9791. 3) Banerdt et al (1982) *J. Geoph. Res. 87*, 9723-9734. 4) Chicarro et al (1985) *Icarus 63*, 153-174. 5) Wichman and Schultz (1987) *Lunar Planet. Sci. Conf. 18*, 1078-1079. 6) Wichman and Schultz (1989) *J. Geoph. Res. 94*, 17333-17357. 7) Schultz and Lutz (1988) *Icarus 73*, 91-141. 8) Melosh (1980) *Icarus 44*, 745-751. 9) Wichman and Schultz (1986) *Lunar Planet. Sci. Conf. 17*, 942-943. 10) Strom et al (1975) *J. Geoph. Res. 80*, 2478-2507. 11) Strom (1978) *Space Sci. Rev. 24*, 3-70. 12) Schultz (1976) *Moon Morphology*.

2. AGE OF RIDGE/SCARP SYSTEMS

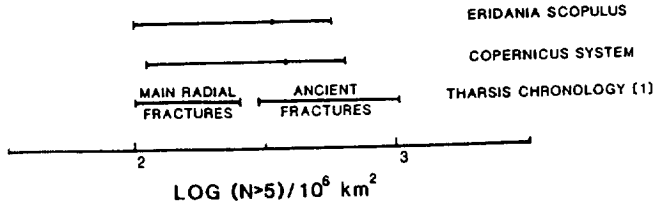

Figure 2. Crater ages derived from linear crater counts (6) for the scarp/ridge systems compared to the Tharsis tectonic history of Wise et al (1).